

Conjugated Polymer with Rigid Donor Poly(*para*-divinylphenylamino) Backbone and Pendant Cyanoacetic Acid Acceptor for Dye Sensitized Solar Cells

Zhen Fang,¹ Danlu Wu,² Shahar Keinan,¹ Bin Liu³

¹Department of Chemistry, University of North Carolina, Chapel Hill, North Carolina 27599

²Department of Chemistry, Tufts University, Medford, Massachusetts 02155

³Department of Chemical and Biomolecular Engineering, National University of Singapore, 4 Engineering Drive 4, Singapore 117576

Correspondence to: Z. Fang (E-mail: Fangzh78@unc.edu)

Received 24 May 2014; accepted 12 July 2014; published online 6 August 2014

DOI: 10.1002/pola.27334

ABSTRACT: A donor backbone [poly(*para*-divinylphenylamino)]-acceptor (cyanoacetic acid side group) type conjugated polymer (**P2**) has been synthesized and used as the active material for dye-sensitized solar cells. DFT calculation shows that the insertion of vinyl link in the polymer backbone leads to a planar structure in **P2** and changes the excited state significantly. Photoelectrochemical cells based on the DSSC format were fabricated using the polymers as sensitizers. The cell con-

structed using **P2** exhibits a considerably high peak IPCE and J-V response, with an overall power conversion efficiency of 3.67%. © 2014 Wiley Periodicals, Inc. *J. Polym. Sci., Part A: Polym. Chem.* **2014**, *52*, 2958–2965

KEYWORDS: conjugated polymer; dye sensitized solar cell; structure-property relation; thin film

INTRODUCTION Taking advantages of relatively low manufacturing cost and capability of large scale production on flexible substrates,^{1,2} dye-sensitized solar cells (DSSCs) have been regarded as the most promising alternative to conventional inorganic photovoltaic cells, for example, silicon,³ CIGS, and CdTe.⁴ A typical DSSC is composed of a TiO₂ photoanode sensitized by a transition metal complex, such as Ru complexes, accomplishing maximum power conversion efficiencies (PCE) up to ~11%.⁵ A record efficiency of 12.3% was recently achieved using a zinc porphyrin with Co^(II/III) tris(bipyridyl) as the electrolyte.⁶ Nevertheless, several critical disadvantages, for example, high cost materials (noble metals) and environmental safety issue of heavy metals, prompt the research of metal-free organic chromophores with donor-acceptor (D-A) structures.^{7,8} Currently, DSSCs with pure organic dyes have comparable PCEs (~10%).^{9–11}

Within the large number of organic materials for photovoltaic application, conjugated polymers (CPs) with D-A structure have been extensively developed as active materials in bulk heterojunction solar cells.^{12–14} However, CP sensitizers in DSSCs are much less discussed.¹⁵ Such CPs feature strong light harvesting, excellent electron-hole dissociation, and multiple anchoring functionalities, all of which are crucial

elements for high DSSC efficiency. In particular, CPs with main-chain donor and side-chain acceptor structure exhibit high efficiencies in DSSCs.^{16,17} Interest on tuning the donor/acceptor pair and further questions on understanding the structure-property relationship led us to design novel CPs, while maintaining the D-A motif. Specifically, we previously designed a poly(triphenylamines) (**P1** in Chart 1) with cyanoacetic acid side group and thiophenyl as the link, which shows strong charge separation at the excited states and favors electron injection to semiconductor, that is, TiO₂.¹⁸ This design led to a high efficient polymer DSSCs with a PCE of ~3.4%. Nevertheless, the light absorption band remained narrow due to the twisted phenyl-phenyl backbone structure. In this presentation, an improvement on the previous design is tested, by inserting a vinyl link between two triphenylamines (**P2** in Chart 1). This stilbene derivative features a planar structure and is more favorable for extending conjugation. We describe here the synthesis and characterization of **P2**. A detailed computational model is presented for the charge separation states, showing enhanced intramolecular charge transfer (ICT) characters for **P2**. **P2** was also fabricated as the active materials in DSSC, with broader external action efficiencies. Another consideration was that polymer size significantly affects dye adsorption onto TiO₂

Additional Supporting Information may be found in the online version of this article.

© 2014 Wiley Periodicals, Inc.

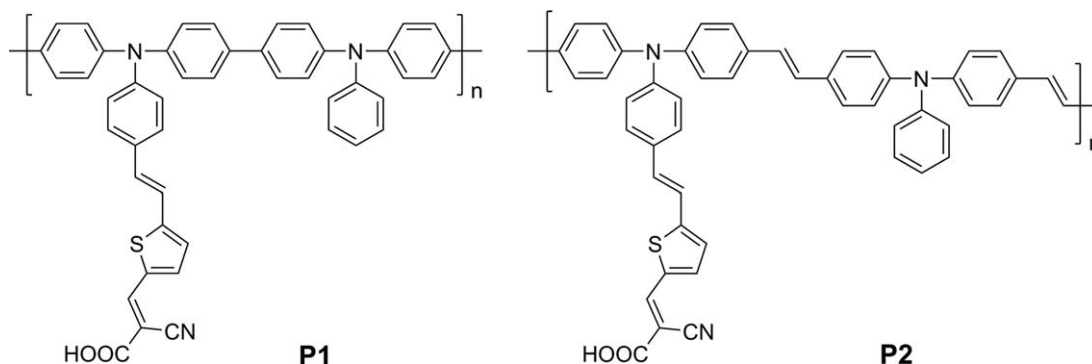


CHART 1 Structures of P1 and P2.

particles due to the difficulty for larger size polymers diffusing through the nanoscale pores in TiO₂ film. Thus, in the present research, we carefully controlled the degree of polymerization (DP) to ensure effective polymer adsorption on films and optimized PCE.

EXPERIMENTAL

Materials and Synthesis

All reagents were used as received unless otherwise specified. Toluene was distilled from sodium/benzophenone. Triethylamine was refluxed with calcium hydride and distilled. DMF was stirred with calcium hydride and distilled under reduced pressure. 5-(4-(Bis(4-bromophenyl)amino)styryl)thiophene-2-carbaldehyde was synthesized according to previous report.¹⁸ *N,N'*-bis(4-bromophenyl)aniline, tributyl(vinyl)tin, bis(triphenylphosphine)palladium chloride, palladium acetate, tris(4-vinylphenyl)phosphine, cyanoacetic acid, and piperidine were used as received from Sigma-Aldrich. Chloroform, acetonitrile and other solvents were purchased from Fisher Scientific. All reactions were carried out under nitrogen or argon flow unless otherwise noted.

General Methods and Instrumentation

NMR spectra were obtained on a Bruker instrument operating at 400 MHz with chloroform-*D* and/or DMSO-*D*₆ as solvents. The molecular weight was measured by GPC and calibrated by polystyrene standards with DMF as the solvent. UV-vis absorption spectra were recorded on a Hewlett Packard 8453 spectrophotometer. Emission spectra were recorded on an Edinburgh Instruments FLS920 emission spectrometer, equipped with a Xenon light; the spectra are corrected for instrument response. Excitation was at 400 nm, with inclusion of a 450 nm long-pass optical filter before the detector. Cyclic voltammetry (CV) was carried out on a computer-controlled CHI660D electrochemical workstation, where a glassy carbon electrode served as the working electrode, a platinum electrode as the counter electrode, and a Ag/AgNO₃ as the reference electrode. Ferrocene (Fc) was used as an external reference. A solution of tetrabutylammonium hexafluorophosphate (0.1 M) in dry DMF was used as the supporting electrolyte, and the scan rate was 100 mV s⁻¹.

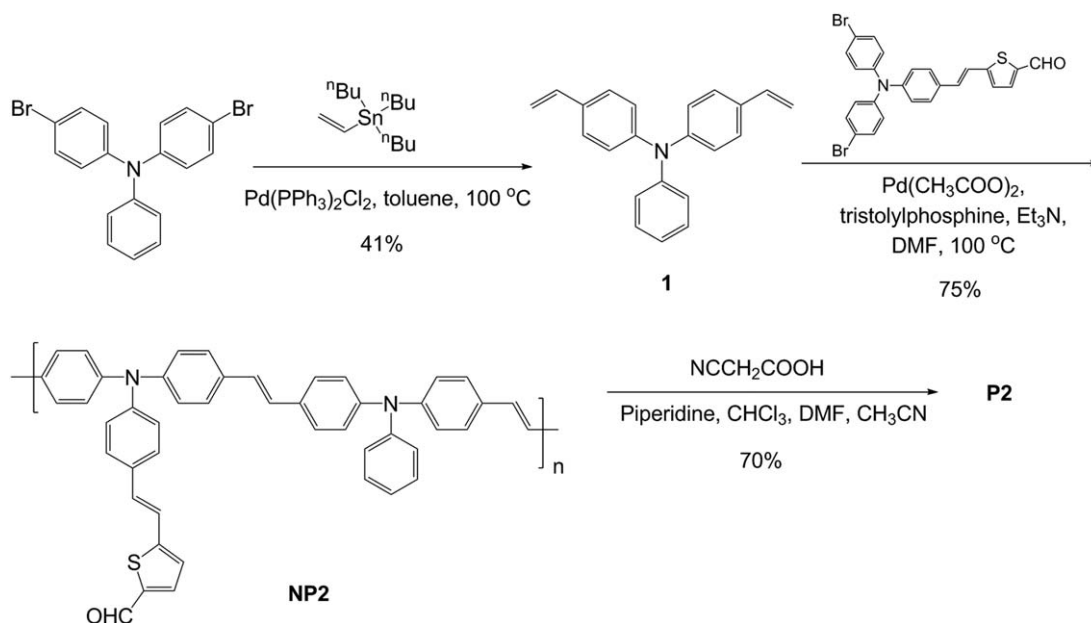
DSSC Fabrication and Characterization

The cells were fabricated as a sandwich with fluorine doped tin(IV) oxide (FTO) conducting glass, nanocrystalline TiO₂ as the wide band-gap semiconductor with the dyes adsorbed, I⁻/I₃⁻ electrolyte for charge regeneration and a Pt counter electrode as a catalyst. The TiO₂ paste, which was purchased from Solaronix® was doctor-bladed onto a clean FTO glass slide and sintered at 450 °C for 30 min. The sintered electrode was immersed into the polymer solution in DMF [\sim 0.2 mM, based on repeat units (RU)] for 24 h to allow for dye adsorption. The counter electrode was prepared using the reported method from drop-casting a solution of H₂PtCl₆ (2 mg in 1 mL ethanol) followed by heat treatment at 400 °C for 15 min.¹⁹ Finally, an electrolyte solution containing 0.03 M I₂, 0.05 M LiI, 0.1 M guanidinium thiocyanate, 1 M 1,3-dimethyl imidazolium iodide, and 0.5 M tert-butylpyridine in a mixture of acetonitrile and valeronitrile (volume ratio = 85:15) was injected. The device was assembled and sealed according to the literature.²⁰ The active area of the cell was \sim 0.28 cm².

The current-voltage characteristics of the cells were measured with a Keithley 2400 source meter under AM1.5 (100 mW/cm²) solar simulator. For IPCE measurements, the cells were illuminated by monochromatic light from an Oriel Cornerstone spectrometer, and the current response under short circuit conditions was recorded at 10 nm intervals using a Keithley 2400 source meter. The light intensity at each wavelength was calibrated with an energy meter (S350, UDT Instruments).

Computational Methods

All molecular geometries were calculated by density functional theory (DFT) with the B3LYP functional and the 6-31G** basis set.²¹ Solvent environment effects were described by using the polarizable continuum model with the integral equation formalism variant for DMF. Tighter convergence criteria and a more accurate numerical integration grid were specified, to ensure finding the exact geometrical minima. Frequencies were calculated and checked to make sure that all frequencies were positive. Electronic spectra were calculated using TD-DFT, based on the procedure



previously outlined by Jacquemin et al.²² The geometry-optimized structures were used in the TD-DFT calculations, with the PBE0 functional,²³ and the same basis-set and solvent effects as in the geometry optimization. The adiabatic approximation of time dependent DFT was used to solve for 60 singlet excited states.²⁴ All calculations were done in Gaussian 09, Revision C.01.²⁵

N,N'-Bis(4-vinylphenyl)benzenamine (**1**)

A mixture containing *N,N'*-bis(4-bromophenyl)aniline (0.5 g, 1.24 mmol), tributylvinyltin (2 mL, 6.70 mmol), 2,6-di-*tert*-butylphenol (0.020 g, 0.10 mmol), Pd(PPh₃)₂Cl₂ (0.035 g, 0.05 mmol), and toluene (10 mL) was bubbled with argon for 20 min, and then stirred overnight at 100 °C under argon. After cooled to room temperature, the mixture was diluted by addition of ether. KF (0.05 g) was added and stirred for 4 h. The mixture was washed with water and dried over anhydrous Na₂SO₄. After the solvent was distilled out under reduced pressure, the crude was purified over silica gel using hexane as the eluent to yield **1** as a yellow oil (0.15 g, 41 %). ¹H-NMR (400 MHz, CDCl₃) δ 7.28–7.21 (m, 6H), 7.09–7.00 (m, 7H), 6.64 (dd, 2H, *J* = 9.6 Hz), 5.63 (d, 2H, *J* = 17.5 Hz), 5.15 (d, 2H, *J* = 10.8 Hz); ¹³C-NMR (100 MHz, CDCl₃) δ 147.19, 136.17, 132.10, 129.22, 127.06, 124.53, 124.34, 123.82, 123.58, 123.12, 122.89, 112.25; Anal. Calcd C₂₂H₁₉N: C, 88.85; H, 6.44; N, 4.71; Found: C, 88.79; H, 6.56; N, 4.65.

NP2

To a solution containing 5-(4-(bis(4-bromophenyl)amino)styryl)thiophene-2-carbaldehyde (0.10 g, 0.18 mmol) and **1** (0.055 g, 0.18 mmol) in DMF (3 mL), previously bubbled with argon for 20 min, palladium acetate (0.002 g, 0.0074 mmol), tris(*o*-tolyl)phosphine (0.011 g, 0.037 mmol), and triethylamine (1 mL) were added. The mixture was stirred

in dark at 100 °C for 5 h. A small amount of dichloromethane was added to dilute the solution. After filtered, the solution was added to diethyl ether to yield **NP2** as a dark red solid (0.092 g, 76%). Further purification was conducted using dissolve-precipitate cycles several times, followed by a size exclusion chromatography using THF as the eluent. ¹H-NMR (400 MHz, CDCl₃) δ 9.83 (s, 1H), 7.64–6.97 (m, 31H). *M_n* = 3500, *M_w*/*M_n* = 1.5.

P2

To a solution containing **NP2** (0.056 g, 0.086 mmol, in RUs), chloroform (10 mL), acetonitrile (1 mL), and DMF (1 mL), cyanoacetic acid (0.020 g, 0.24 mmol), and piperidine (0.5 mL) were added. The mixture was refluxed for 4 h under nitrogen. After the solvent was distilled out under reduced pressure, the residue was dissolved in DMF, filtered and precipitated from acetone to yield **P2** as an orange solid (0.045 g, 73%). ¹H-NMR (300 MHz, CDCl₃) δ 8.25 (br, 1H), 7.62–6.97 (m, 31H); Anal. Calcd (C₄₈H₃₃N₃O₂S)*n*: C, 80.53; H, 4.65; N, 5.87; Found: C, 80.29; H, 4.91; N, 5.90; *M_n* = 3800, *M_w*/*M_n* = 1.5.

RESULTS AND DISCUSSION

The general synthetic route for **P2** is illustrated in Scheme 1. *N,N'*-Bis(4-vinylphenyl)benzenamine (**1**) was synthesized from *N,N'*-bis(4-bromophenyl)aniline and tributyl(vinyl)tin by Stille coupling reaction, with a yield of ~41%. 5-(4-(Bis(4-bromophenyl)amino)styryl)thiophene-2-carbaldehyde was synthesized according to the literature,¹⁸ which was condensed with monomer **1** to yield precursor polymer **NP2** by Heck cross coupling reaction. Following the polymerization reaction, **NP2** was treated with a preparative size exclusion chromatography to remove catalyst and oligomers. The aldehyde group was then functionalized with cyanoacetic

TABLE 1 Properties of Polymers

	M_n	PDI	λ_{abs} (nm) ^a	ϵ ($10^4 \text{ cm}^{-1}\text{M}^{-1}$)	λ_{em} (nm) ^a	ϕ_{fl} ^b
P1 ^c	3100	1.70	372, 445	3.6	615	0.021
P2	3800	1.50	411, 490	3.9	715	0.0025

^a Estimated error in λ max is ± 5 nm.

^b Determined using quinine sulfate in 0.1 M H_2SO_4 as the standard, $\phi_{\text{fl}} = 0.546$.²⁷

^c The properties of **P1** are in well agreement with previous work.¹⁸

acid via Knoevenagel condensation reaction in the presence of piperidine as the catalyst. The condensation was monitored by UV-vis absorption spectroscopy (see Fig. S1 in the Supporting Information). The rising absorption band at 490 nm as a result of ICT characteristic indicates the appearance of cyanoacetic acid; while the neutral precursor **NP2** shows a single π - π^* transition band at ~ 420 nm corresponding to the backbone and the thiophene side chains. A detailed electronic state delocalization study will be discussed later in the calculation section.

The molecular weight and polydispersity index (PDI) was determined by analytical GPC using polystyrene standards. The number average molecular weight (M_n) of **P2** is 3800, with a PDI of 1.5 (Table 1). The DP, which is ~ 5 , was calculated from the formula weight of the RU and M_n . This DP suggests the phenylene RU number of about 20, which is similar to **P1**, and in agreement with the literature reported optimal chain length for effective adsorption onto nanoporous TiO_2 .²⁶ The $^1\text{H-NMR}$ spectrum of **P2** after Knoevenagel condensation does not show the protons of $-\text{CHO}$ (~ 9.80 ppm) in **NP2**, consistent with complete deprotection.

The absorption and emission spectra of **P2** were measured in DMF solution. The spectra are shown in Figure 1, and a tabulation of absorption and emission maxima, extinct coefficient (ϵ) values, and fluorescence quantum yields (ϕ_{fl}) is provided in Table 1. The polymer concentration is calculated based on the RU. For comparison, the absorption and emission spectra of **P1** are also included. Both polymers feature two-band absorption, where the long wavelength band corresponds to an ICT from the electron-rich (triphenylamines-vinyl-thiophene) segments to the electron-deficient (cyanoacetic acid) unit, and the high energy band corresponds to the π - π^* transition of backbones. This character is typical for donor-acceptor CPs and has been discussed.²⁸ We note that the π - π^* transition band of **P2** red-shifts by ~ 40 nm relative to that of **P1**, indicating an extended conjugation backbone in **P2**. Meanwhile, a comparable redshift in the ICT band of **P2** relative to **P1** is observed, which will be discussed in details later in the calculation section. Another distinct observation in the absorption spectra is that the extinct coefficient of **P2** ($3.9 \times 10^4 \text{ cm}^{-1}\text{M}^{-1}$ at 490 nm) increases by 10% relative to that of **P1** ($3.6 \times 10^4 \text{ cm}^{-1}\text{M}^{-1}$ at 445 nm), which suggests larger light harvesting capability for **P2**.

P2 exhibits weak red fluorescence with $\lambda_{\text{max}} = 715$ nm, while **P1** exhibits relatively strong fluorescence with $\lambda_{\text{max}} = 615$ nm. The significant redshift of emission for **P2**, suggests a much

lower excited state relative to **P1**, which is in agreement with the shift in absorption spectra. Both **P1** and **P2** feature large Stokes shifts of ~ 200 nm. These large Stokes shifts suggest significant energy loss upon excitation, which is likely due to the ICT and/or the twisted polymer backbone (**P1**). The fluorescence quantum yields decrease significantly from **P1** (2.1%) to **P2** (0.25%). Normally, this dramatic decrease is likely due in part to narrowed energy gap resulting in increased nonradiative decay for **P2**.²⁹

To better understand the structure-property relationship in **P1** and **P2**, we have calculated the frontier orbitals of the **P1** and **P2** RUs. Our previous calculation in a single **P1** monomer suggests a significantly efficient charge separation upon excitation.¹⁸ However, in the previous calculation a possible significant interaction from the approximate neighbor units was omitted. In order to overcome this, we present here calculations for two RUs, that is, ABAB type, instead of a single monomer. These calculations were conducted on DFT optimized geometry, as specified in the methods section. The optimized molecular structures of both **P1** and **P2** are shown in Figure 2. The connecting two triphenylamines in **P1** are twisted, while those in **P2** are planar and transconfiguration, indicating an extended conjugation that is larger than **P1**, accounting for the redshift (~ 40 nm) in the π - π^* transition band in UV-vis spectra. For each optimized geometry, we calculated the ground-state electronic transition using TD-DFT (details can be found in the Methods section) and determined the orbitals that contributed to these transitions.

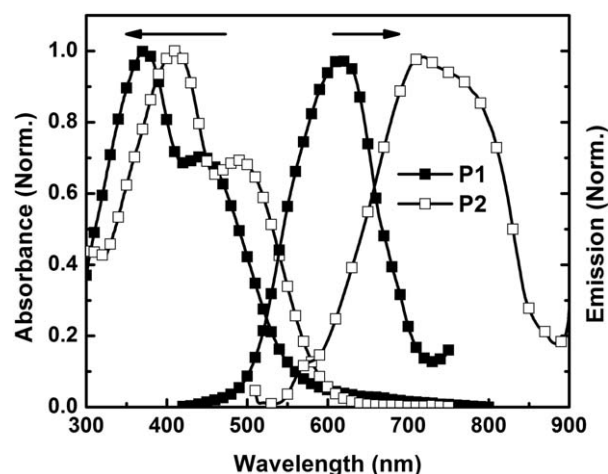


FIGURE 1 Normalized absorption and emission spectra of **P1** and **P2** in DMF solution, [RU] = 10 μM .

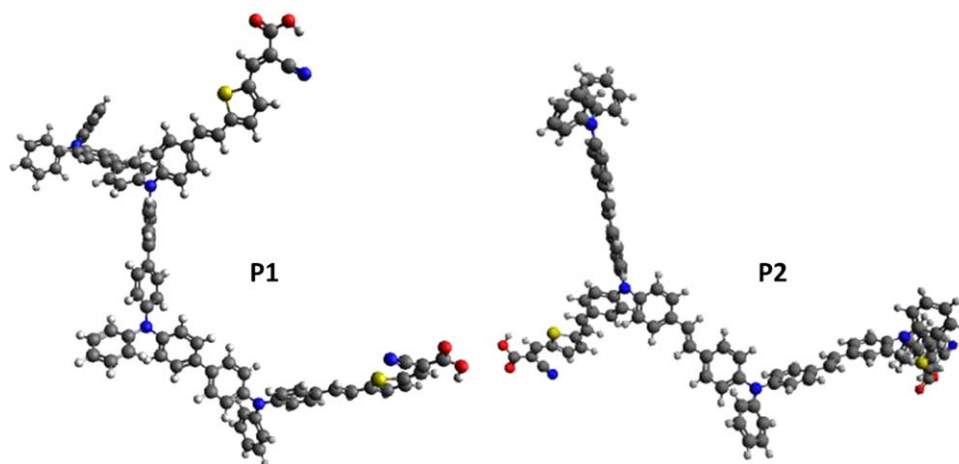


FIGURE 2 Optimized molecular structures of **P1** and **P2**, two RUs are illustrated. Black: Carbon; Gray: Hydrogen; Blue: Nitrogen; Red: Oxygen; Yellow: Sulfur. [Color figure can be viewed in the online issue, which is available at wileyonlinelibrary.com.]

We show here, Figure 3, the contributing orbitals for the strongest excitations from the high (3.22 eV for **P1**, 2.68 eV for **P2**, HOMO to LUMO+2, +4 transition) and low (1.89 eV for **P1**, 1.72 eV for **P2**, HOMO to LUMO transition) energy transition, see also Supporting Information. For both polymers, the HOMO electrons are mainly localized at the triphenylamines backbones; while small amount is delocalized at the thiophene-vinyl-cyanoacetic acid in **P2**. A valuable note is that both HOMOs are most localized at central three triphenylamines, likely suggesting an effective conjugation length.³⁰ The high energy $\pi \rightarrow \pi^*$ transition in **P2** is from orbitals HOMO to LUMO+2 and has a better overlap with stronger oscillator strength (2.04) than that in **P1**, which corresponds to HOMO to LUMO+2 and LUMO+4 with weaker oscillator

strength (1.49). The low energy transition is also a $\pi \rightarrow \pi^*$ transition, Figure 3, lower part. For both polymers, the LUMO orbital is completely localized on the side groups, i.e. vinyl-thiophene-vinyl-cyanoacetic acid. It demonstrates an effective charge separation once the molecules are excited. It is in agreement with the measured ICT band in absorption spectra. The excited states of **P2** are equally delocalized on each side chains, suggesting a better charge separation than those of **P1**. This pronounced intramolecular charge separation favors electron injection from polymer to an *n*-type semiconductor, for example, TiO₂.

Polymer DSSC device was fabricated as a sandwich of sensitized TiO₂ photoanode, electrolyte solution and Pt counter

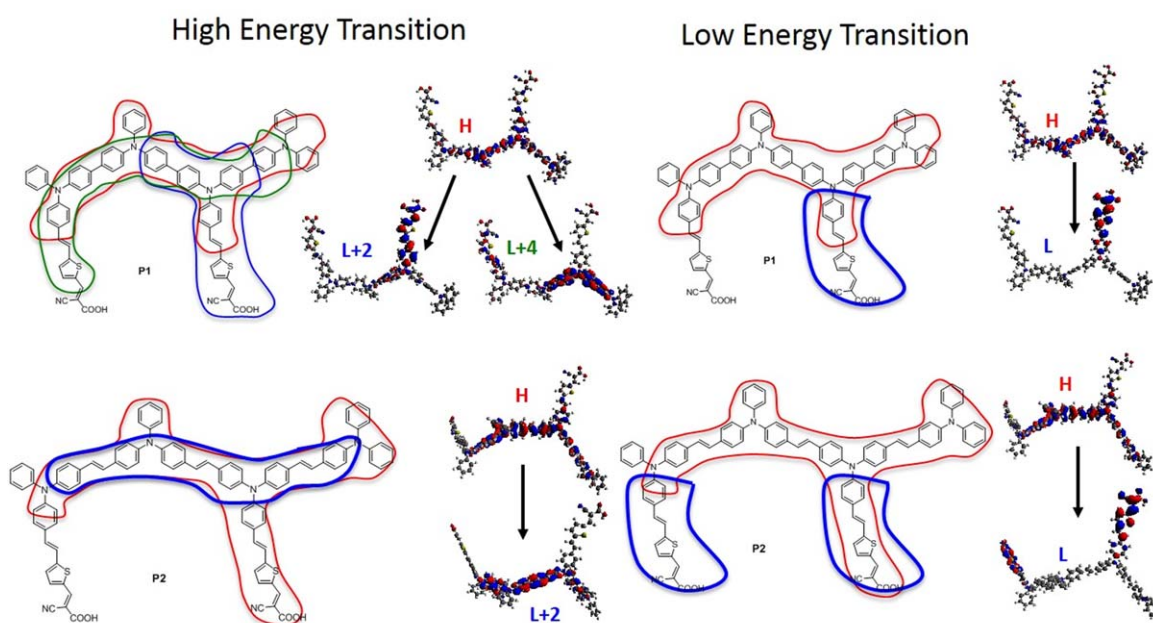


FIGURE 3 Calculated frontier orbitals for **P1** (top) and **P2** (lower) RUs for the high and low energy transition. [Color figure can be viewed in the online issue, which is available at wileyonlinelibrary.com.]

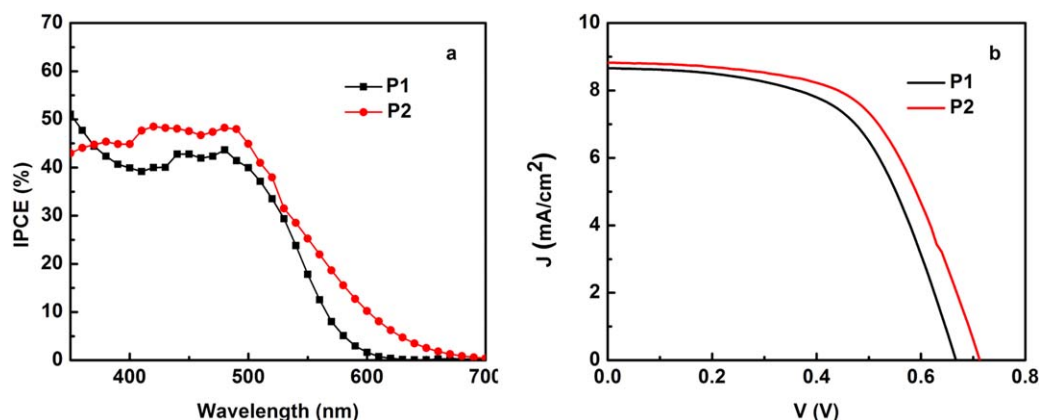


FIGURE 4 Photocurrent action spectra (a) and J - V characteristics (b) of two typical cells made from **P1** and **P2**, selected from three comparable devices each. [Color figure can be viewed in the online issue, which is available at wileyonlinelibrary.com.]

electrode. The electrolyte solution contains 0.03 M I_2 , 0.05 M LiI, 0.1 M guanidinium thiocyanate, 1 M 1,3-dimethyl imidazolium iodide, and 0.5 M tert-butylpyridine in a mixture of acetonitrile and valeronitrile (volume ratio, 85:15). For each polymer, three devices have been fabricated and tested to affirm the reproducibility. The fabrication and test conditions are described in details in the Supporting Information. Herein, we show the typical performance as shown in Figure 4. Figure 4(a) illustrates the photocurrent action spectra (IPCE) of the polymer sensitized solar cells obtained using monochromatic illumination under short circuit conditions.

The electrochemical properties of two polymers were characterized using CV method in anhydrous and degassed DMF solution (See Fig. S2 in the Supporting Information). The redox values were listed in Table 2, where E_{ox} is the oxidation potential of the ground state. The HOMO energy is estimated by the equation, $HOMO = -E_{ox}$ versus $Fc/Fc^+ - 5.1$ eV, where the Fc/Fc^+ redox couple is ~ -5.1 eV versus vacuum in the Fermi scale.³¹ This estimation has been established to determine the energy levels of donor-acceptor polymers by CV.³² Assuming the electron injection occurs after a relaxed excited state, the LUMO energy is estimated as the oxidation potential of relaxed state, $E_{ox}^* = E_{ox} - E_{0-0}$, where $E_{0-0} = 1240/\lambda_{em}$, estimated from the emission maximum. The similar oxidation potential is in agreement with their similar HOMO calculated localization at triphenylamines backbones, and sufficiently more negative than the redox potential of the iodine/iodide couple (-4.95 eV),³³ for the photo-oxidized polymers efficiently reduced by iodide. Although the lower LUMO level of **P2** is in part due to

the delocalization at more acceptors, as shown in Figure 3, both LUMO values are still positive compared to the TiO_2 conduction band ($E_{CB} = -3.9$ eV),³⁴ for charge injection into the semiconductor.

Figure 4(a) shows the IPCE spectrum of **P2** has broader absorption relative to that of **P1**, which is consistent to that seen in the polymers' absorption spectra (Fig. 1). In particular, the DSSC cell fabricated with **P1** has a peak external quantum efficiency of about 40%, whereas the cells from **P2** have a maximum IPCE value of 50%, indicating that at short circuit condition **P2** gives rise to a more efficient external quantum yield than **P1**, which is in part due to the increased extinct coefficient of **P2**. The current-voltage (J - V) characteristics under AM1.5 illumination (100 mW cm^{-2}) of the polymer sensitized DSSCs are shown in Figure 4(b). The performances of the cells in terms of short-circuit current density (J_{sc}), open-circuit voltage (V_{oc}), fill factor (FF) and overall PCE (η_{cell}) are summarized in Table 3, along with the maximum IPCE values. The photovoltaic parameters (J_{sc} , V_{oc} , FF, and η_{cell}) of the cell made from **P1** are 8.66 mA cm^{-2} , 0.66 V, 0.58, and 3.30%. In contrast, the cell made from **P2** has enhanced performance. J_{sc} , V_{oc} , FF, and η_{cell} of **P2** are 8.82 mA cm^{-2} , 0.70 V, 0.59, and 3.67%, respectively.

In particular, the short-circuit current density is proportional to the light harvesting efficiency (LHE) and electron injection efficiency (Φ_{inj}). While the larger absorption coefficient of **P2** contributes to an enhanced LHE, Φ_{inj} is proportional to the driving force of injection, which is representative to the difference between the relaxed excited state energy level of polymers (E_{ox}^*) and the E_{CB} of TiO_2 , assuming the electron

TABLE 2 Electrochemical Properties of Polymers

Compound	E_{ox} V vs Fc^+/Fc^a	E_{0-0} (eV) ^b	HOMO (eV)	LUMO (eV)
P1	0.32	2.02	-5.42	-3.40
P2	0.36	1.73	-5.46	-3.73

^a Determined as the onset oxidation in CV spectra.

^b Estimated from emission maximum, $1240/\lambda_{em}$.

TABLE 3 Summary of Solar Cell Characteristics under AM1.5 Illumination

	V_{oc} (V)	J_{sc} (mA/cm ²)	FF (%)	Maximum IPCE (%)	η_{cell} (%)
P1	0.66	8.66	58	42.0	3.30
P2	0.70	8.82	59	50.6	3.67

injection is after the relaxation upon illumination. Apparently, **P2** has a weaker driving force than **P1** due to the more negative LUMO. However, the enhanced extinct coefficient of **P2** relative to **P1** is indicative of a larger LHE. Taking both factors together, there is a small increase in the photocurrent, that is, from 8.66 to 8.82 mA/cm². V_{oc} represents the energy difference between the redox potential of electrolyte and the quasi-Fermi level of TiO₂, while the former remains constant and the latter one shifts due to many factors, for example dipole dependence from different dyes.³⁵ The increased dipole moment of the RU of **P2** relative to that of **P1** due to introduction of vinyl links and the planar backbones may produce an upshift of the quasi-Fermi level and consequently enhance the V_{oc} of the DSSC.

CONCLUSIONS

In conclusion, a donor (triphenylamines backbone)-acceptor (cyanoacetic acid side group) type CP (**P2**) has been synthesized and used as active materials for DSSCs. DFT calculation shows that the HOMO electrons are mainly localized at the approximate three triphenylamine-vinyl and thiophene links, suggesting the effective conjugation length. The twisted backbone in **P1** becomes planar in **P2**. The significant charge transfer state features a dominant low energy transition, and is localized at each thiophene-vinyl-cyanoacetic acid side groups; while polymers without vinyl in the backbone (**P1**) only alternately localize the ICT at every side group. Significant red shift at both π - π^* transition band (high energy) and ICT band in **P2** relative to **P1** leads to an enhanced light harvesting capability.

Photoelectrochemical cells based on the DSSC format were fabricated using the polymers as sensitizers. By carefully controlling the molecular weight of the polymer, a considerable amount of **P2** has been adsorbed on metal oxide. The cell constructed using **P2** exhibits a considerably higher peak IPCE than that using **P1**. The DSSC fabricated with **P2** exhibits enhanced performance, with J_{sc} of 8.82 mA cm⁻², V_{oc} of 0.70 V, FF of 59%, and η_{cell} of 3.67%. In general, the design principle in this study shows that the insertion of vinyl in the backbone results in planar conformation and improved light harvesting. Future work may search for more efficient donor-acceptor couples and study the intrinsic photon excitation, charge separation, and injection.

ACKNOWLEDGMENT

The authors acknowledge support from the Department of Chemical and Biomolecular Engineering, National University of Singapore, and support from the UNC EFRC: Center for Solar Fuels, an Energy Frontier Research Center funded by the U.S. Department of Energy, Office of Science, Office of Basic Energy Sciences under Award Number DE-SC0001011 supporting Z. Fang and S. Keinan.

REFERENCES AND NOTES

- 1 B. O'Regan, M. Grätzel, *Nature* **1991**, *353*, 737–740.
- 2 M. Grätzel, *Inorg. Chem.* **2005**, *44*, 6841–6851.
- 3 M. Konagai, *Jpn. J. Appl. Phys.* **2011**, *50*, 030001.

- 4 K. L. Chopra, P. D. Paulson, V. Dutta, *Prog. Photovolt. Res. Appl.* **2004**, *12*, 69–92.
- 5 Y. Chiba, A. Islam, Y. Watanabe, R. Komiya, N. Koide, L. Han, *Jpn. J. Appl. Phys.* **2006**, *45*, L638–L640.
- 6 A. Yella, H. W. Lee, H. N. Tsao, A. K. Chandiran, M. K. Nazeeruddin, E. W. Diau, C. Y. Yeh, S. M. Zakeeruddin, M. Grätzel, *Science* **2011**, *334*, 629–634.
- 7 H. Li, T. M. Koh, A. Hagfeldt, M. Grätzel, S. G. Mhaisalkar, A. C. Grimsdale, *Chem. Commun.* **2013**, *49*, 2409–2411.
- 8 Q. Feng, Q. Zhang, X. Lu, H. Wang, G. Zhou, Z.-S. Wang, *ACS Appl. Mater. Interfaces* **2013**, *5*, 8982–8990.
- 9 T. Bessho, S. M. Zakeeruddin, C.-Y. Yeh, E. W. Diau, M. Grätzel, *Angew. Chem. Int. Ed.* **2010**, *49*, 6646–6649.
- 10 W. Zeng, Y. Cao, Y. Bai, Y. Wang, Y. Shi, M. Zhang, F. Wang, C. Pan, P. Wang, *Chem. Mater.* **2010**, *22*, 1915–1925.
- 11 B.-G. Kim, K. Chung, J. Kim, *Chem. Eur. J.* **2013**, *19*, 5220–5230.
- 12 J. Hou, H.-Y. Chen, S. Zhang, Y. Yang, Y. Wu, G. Li, *J. Am. Chem. Soc.* **2009**, *131*, 15586–15587.
- 13 W. Ma, C. Yang, X. Gong, K. Lee, A. J. Heeger, *Adv. Funct. Mater.* **2005**, *15*, 1617–1622.
- 14 Y. Li, *Acc. Chem. Res.* **2012**, *45*, 723–733.
- 15 C. Kanimozhi, P. Balraju, G. D. Sharma, S. Patil, *J. Phys. Chem. C* **2010**, *114*, 3287–3291.
- 16 D. W. Chang, S.-J. Ko, J. Y. Kim, S.-M. Park, H. J. Lee, L. Dai, J.-B. Baek, *Macromol. Rapid Commun.* **2011**, *32*, 1809–1814.
- 17 H. Tan, C. Pan, G. Wang, Y. Wu, Y. Zhang, X. Chen, Y. Zou, G. Yu, M. Zhang, *RSC Adv.* **2013**, *3*, 16612–16618.
- 18 W. Zhang, Z. Fang, M. Su, M. Saeys, B. Liu, *Macromol. Rapid Commun.* **2009**, *30*, 1533–1537.
- 19 S. Ito, T. N. Murakami, P. Comte, P. Liska, C. Grätzel, M. K. Nazeeruddin, M. Grätzel, *Thin Solid Films* **2008**, *516*, 4613–4619.
- 20 S. Ito, S. M. Zakeeruddin, R. Humphry-Baker, P. Liska, R. Charvet, P. Comte, M. K. Nazeeruddin, M. Péchy, M. Takata, H. Miura, S. Uchida, M. Grätzel, *Adv. Mater.* **2006**, *18*, 1202–1205.
- 21 (a) A. D. Becke, *J. Chem. Phys.* **1993**, *98*, 5648–5652; (b) C. Lee, W. Yang, R. G. Parr, *Phys. Rev. B Condens. Matter* **1988**, *37*, 785–789.
- 22 (a) D. Jacquemin, E. A. Perpète, G. E. Scuseria, I. Ciofini, C. Adamo, *J. Chem. Theory Comput.* **2008**, *4*, 123–135; (b) D. Jacquemin, J. Preat, E. A. Perpète, C. Adamo, *Int. J. Quantum Chem.* **2010**, *110*, 2121–2129.
- 23 (a) J. P. Perdew, K. Burke, M. Ernzerhof, *Phys. Rev. Lett.* **1996**, *77*, 3865–3868; (b) C. Adamo, V. Barone, *J. Chem. Phys.* **1999**, *110*, 6158–6170.
- 24 R. Bauernschmitt, R. Ahlrichs, *Chem. Phys. Lett.* **1996**, *256*, 454–464.
- 25 M. J. T. Frisch, G. W. Trucks, H. B. Schlegel, G. E. Scuseria, M. A. Robb, J. R. Cheeseman, G. Scalmani, V. Barone, B. Mennucci, G. A. Petersson, H. Nakatsuji, M. Caricato, X. Li, H. P. Hratchian, A. F. Izmaylov, J. Bloino, G. Zheng, J. L. Sonnenberg, M. Hada, M. Ehara, K. Toyota, R. Fukuda, J. Hasegawa, M. Ishida, T. Nakajima, Y. Honda, O. Kitao, H. Nakai, T. Vreven, J. A. Montgomery Jr., J. E. Peralta, F. Ogliaro, M. Bearpark, J. J. Heyd, E. Brothers, K. N. Kudin, V. N. Staroverov, R. Kobayashi, J. Normand, K. Raghavachari, A. Rendell, J. C. Burant, S. S. Iyengar, J. Tomasi, M. Cossi, N. Rega, J. M. Millam, M. Klene, J. E. Knox, J. B. Cross, V. Bakken, C. Adamo, J. Jaramillo, R. Gomperts, R. E. Stratmann, O. Yazyev, A. J. Austin, R. Cammi, C. Pomelli, J. W. Ochterski, R. L. Martin, K. Morokuma, V. G. Zakrzewski, G. A. Voth, P. Salvador, J. J. Dannenberg, S. Dapprich, A. D. Daniels, Ö.

- Farkas, J. B. Foresman, J. V. Ortiz, J. Cioslowski, D. J. Fox. Gaussian 09, Revision C.01; Gaussian, Inc.: Wallingford, CT, **2009**.
- 26** Z. Fang, A. A. Eshbaugh, K. S. Schanze, *J. Am. Chem. Soc.* **2011**, *133*, 3063–3069.
- 27** W. H. Melhuish, *J. Phys. Chem.* **1961**, *65*, 229–235.
- 28** P. M. Beaujuge, C. M. Amb, J. R. Reynolds, *Acc. Chem. Res.* **2010**, *43*, 1396–1407.
- 29** J. R. Lakowicz, Principles of Fluorescence Spectroscopy, 3rd ed.; Springer: New York, **2006**.
- 30** M. Wohlgenannt, X. M. Jiang, Z. V. Vardeny, *Phys. Rev. B* **2004**, *69*, 241204.
- 31** C. M. Cardona, W. Li, A. E. Kaifer, D. Stockdale, G. C. Bazan, *Adv. Mater.* **2011**, *23*, 2367–2371.
- 32** (a) P. M. Beaujuge, J. Subbiah, K. R. Choudhury, S. Ellinger, T. D. McCarley, F. So, J. R. Reynolds, *Chem. Mater.* **2010**, *22*, 2093–2106; (b) Y. Zou, A. Najari, P. Berrouard, S. Beaupre, B. R. Aich, Y. Tao, M. Leclerc, *J. Am. Chem. Soc.* **2010**, *132*, 5330–5331.
- 33** F. Lenzmann, J. Krueger, S. Burnside, K. Brooks, M. Gratzel, D. Gal, S. Ruhle, D. Cahen, *J. Phys. Chem. B* **2001**, *105*, 6347–6352.
- 34** A. Hagfeldt, M. Gratzel, *Chem. Rev.* **1995**, *95*, 49–68.
- 35** T. Marinado, K. Nonomura, J. Nissfolk, M. K. Karlsson, D. P. Hagberg, L. Sun, S. Mori, A. Hagfeldt, *Langmuir* **2010**, *26*, 2592–2598.